# Supporting Information

## Electrolyte Dependent HER Activity of Mesoporous Iron-based ZIF-67 Leaf-like Nanosheets

Muhammad Faisal Iqbal[a, b], Mengjiao Li[a], Tao Xu[a], Junchao Lou[a], Weitao Wang[a], Jing Zhang[a]*, Enlai Hu[a]*, Pan Xu[c]*

[a] Key Laboratory of the Ministry of Education for Advanced Catalysis Materials, College of Chemistry and Materials Science, Zhejiang Normal University, Jinhua, 321004 People's Republic of China
[b] Department of Physics, Emerson University Multan, Pakistan
[c] Zhejiang Fenergy Technology Co., Ltd., Pinghu, 314200 People's Republic of China

E-mail: jingzhang@zjnu.edu.cn (Jing Zhang); huenlai@zjnu.edu.cn (Enlai Hu); Pan Xu (xupan@fenergy.com.cn)

## 1. Physical and Electrochemical Characterization

Synthesized products were confirmed using the X-ray Diffractometer (XRD, model; D8-advances), Fourier transform Infrared spectrometer (FTIR, model; Agilent carry 630) and X-ray photoelectron spectroscopy (XPS, model: ESCALAB 250Xi). Morphology and shapes were studied using scanning electron microscopy with an EDX detector (SEM: GeminiSEM 300, EDX: JED-2300T) and high-resolution transmission electron microscopy (TEM and HRTEM, model: JEOL JEM-F200). Surface area, porosity and electrical conductivity were measured using the Brunauer-Emmett-Teller Method (BET; model- Nova Station A) and the electrical conductivity meter with DJS-1D Platinum black conductivity electrode (DDSJ-308F), respectively.

### 1.1 Electrochemical measurements

Electrochemical measurements for the HER process have been measured using the three electrodes electrochemical system (CHI760E), which consists of a reference (Ag/AgCl), counter (carbon rod) and prepared reference electrodes (working electrodes). Electrochemical measurements have been examined in different electrolytes *i. e.* alkaline; 1 M KOH (pH = 13.81), acidic; 0.5 M $H_2SO_4$ (pH = 0.48) and neutral; seawater (pH = 7.98). Working electrodes were prepared on the nickel foam (NF) substrate. Nickel foam (1.2 cm × 0.5 cm) was washed with 1 M HCl to create the hydrophilic features and ethanol and dried at 60 ˚C for 24 hours. The paste of the synthesized product was prepared in ethanol (10 mL) and Nafion binder (50 µL) and deposited on the NF by drop casting. The prepared NF electrodes were dried at 60 ˚C for 24 hours and net deposited mass was found as 1.6 mg on each NF piece.

Linear sweep voltammetry (LSV) was executed in the potential window of 0 to -2 $V_{Ag/AgCl}$ and collected data was transformed into $V_{RHE}$ for the measurement of overpotential (η) and further analysis, using Eq. S1. Tafel slopes were measured using Eq. S2 from the linear part of the corresponding LSV curves. Turnover frequency (TOF) has been extracted at 0.8 $V_{RHE}$ using Eq.S3. Electrochemical surface area (ECSA) has been extracted using Eq. S4. Electrochemical impedance spectroscopy (EIS) was executed in the frequency range of 0.1 to $10^5$ Hz at 10 mV. Equivalent fitting and analysis were carried out for the measurement of $J_{exc}$, electrochemical solution ($R_s$) and charge transfer resistance ($R_{ct}$) ZSimpWin software. $J_{exc}$, was measured using Eq. S5.

LSV collected data was converted into reversible hydrogen potential ($V_{RHE}$) using Eq. S1 and further analysis and HER parameters were evaluated from the converted data.

$$V_{RHE} = \left[E_{Ag/AgCl} + E^{\circ}_{Ag/AgCl} + (pH * 0.059)\right] \qquad (S1)$$

Where $E^{\circ}_{Ag/AgCl}$ is the absolute thermodynamic potential of the Ag/AgCl (0.197 V) and $E_{Ag/AgCl}$ is the measured potential during LSV testing. The pH of the electrolytes and correction factor (0.059) have also been used. Tafel slopes for the HER process were measured from the linear part of the corresponding LSV curves, which satisfies Eq. S2,

$$\eta = a + \left(\frac{2.303 * RT}{\alpha n F}\right) * log\ j \qquad (S2)$$

In Eq. S2, α and n represent the charge transfer coefficient and involved number of electrons. F, T and R correspond to the Faraday constant (96,485 A s $mol^{-1}$), thermodynamic temperature and universal gas constant. Factor 2.303*RT/αnF represents the Tafel slope. Turnover frequency (TOF) has been extracted at the fixed $V_{RHE}$ of 700 $mV_{RHE}$ using Eq. S3. Electrochemical surface area ($A_{ECSA}$) has been extracted using Eq. S4,

$$TOF = \frac{jA}{2n * F} \qquad (S3)$$

$$A_{ECSA} = \frac{C_{dl}}{C_s} \qquad (S4)$$

In Eq. S3, j is the current density measured during LSV testing at a fixed $V_{RHE}$ of 700 $mV_{RHE}$ and A is the area of the substrate. Double-layered capacitance ($C_{dl}$) in Eq. S4 is extracted from the cyclic voltammetry curves (CV). The general specific capacitance ($C_s$) is usually considered in the range of 20-60 µF $cm^{-2}$, which depends on the surface of the substrates.[1, 2] Herein, $C_s$ has been considered due to the flat surface of the substrate. Electrochemical impedance spectroscopy (EIS) was performed in the frequency range of 0.1 to $10^5$ Hz at the amplitude of 10 mV. Exchange current density ($J_{exc}$) was measured from the fitting and analysis of EIS data using the Zsimpwin software. $J_{exc}$, electrochemical solution ($R_s$) and charge transfer resistance ($R_{ct}$) were measured from the Nyquist data using Eq. S5,

$$J_{exc} = \frac{RT}{nAFR_{ct}} \qquad (S5)$$

In Eq. S5, A and $R_{ct}$ are the area of the substrate and charge transfer resistance from the Nyquist fitting data.

## 2. Structural analysis

Structural analysis of the Fe@ZIF-67-1 was carried out using the X-ray Diffractometer (XRD, model; D8-advances). XRD pattern in the 2θ range of 5-60˚ reveals that Fe@ZIF-67-1 exhibited similar peak positions to Fe@ZIF-67-2 structure. The electrocatalyst, Fe@ZIF-67-1 showed peaks at 2θ of 6.86, 12.30, 15.87, 17.86, 21.18, 23.83, 26.10, 32.00, 33.26, 34.94, 36.60, 40.00, 41.04, 53.23 and 58.91˚ and their corresponding d values are mentioned in Table S1 (Fig. S1). The XRD spectrum matches the literature well and corresponds to the successful synthesis of Fe@ZIF-67-1 and Fe@ZIF-67-2 structure.[3-5]

**Table S1.** Summary of XRD peaks and corresponding d values.

| **Fe@ZIF-67-1** | **d values Å** | **Fe@ZIF-67-2 structures** | **d values Å** |
|---|---|---|---|
| 6.86 | 12.8748 | 6.86 | 12.8748 |
| 12.3 | 7.19234 | 8.12 | 10.8799 |
| 15.87 | 5.57986 | 12.12 | 7.29451 |
| 17.86 | 4.96231 | 15.40 | 5.74894 |
| 21.18 | 4.19097 | 19.19 | 4.62143 |
| 23.83 | 3.73099 | 20.03 | 4.42956 |
| 26.10 | 3.41143 | 20.87 | 4.25298 |
| 32.00 | 2.79459 | 24.80 | 3.58713 |
| 33.26 | 2.69147 | 26.10 | 3.41143 |
| 34.94 | 2.56587 | 26.93 | 3.30814 |
| 36.60 | 2.45326 | 28.20 | 3.16215 |
| 40.00 | 2.25221 | 29.88 | 2.98786 |
| 41.04 | 2.19753 | 31.50 | 2.83782 |
| 53.23 | 1.71735 | 33.25 | 2.69232 |
| 58.91 | 1.56648 | 35.14 | 2.55151 |
| | | 36.40 | 2.46622 |
| | | 39.60 | 2.27402 |
| | | 41.65 | 2.16681 |
| | | 43.54 | 2.07695 |
| | | 46.28 | 1.96015 |
| | | 47.33 | 1.91903 |
| | | 50.48 | 1.80652 |
| | | 51.74 | 1.76541 |
| | | 53.00 | 1.72636 |

| | | |
|---|---|---|
| | 57.20 | 1.60915 |
| | 59.10 | 1.56184 |

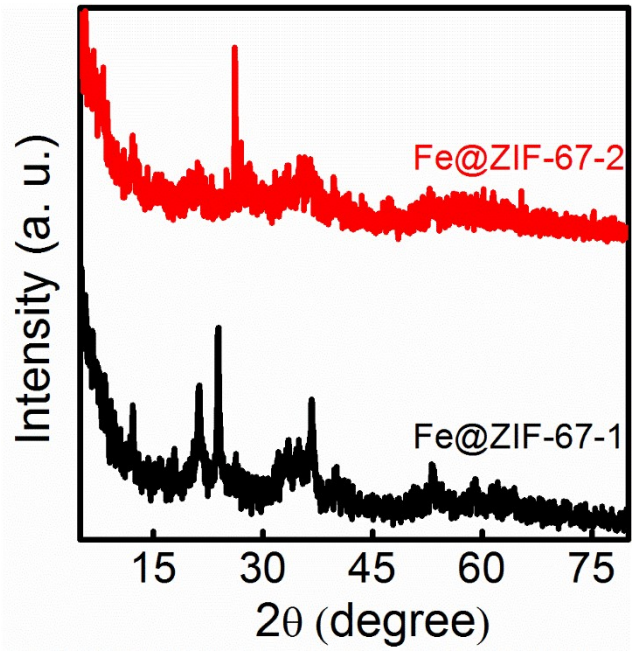


**Fig. S1.** Conventional XRD pattern Fe@ZIF-67-1 structure.

The iron elemental spectrum of Fe@ZIF-67-1 showed binding energy peaks at 710.28, 712.38, 718.33, 724.70, and 732.83 eV (Fig. S2a). The binding energy peaks appeared at 710.28 and 724.70 eV corresponding to the Fe-$2p_{3/2}$ and Fe-$2p_{1/2}$ states of Fe(II), respectively.[6, 7] Meanwhile, the binding energy peaks appeared at 712.38 and 732.83 eV, which correspond to the Fe-$2p_{3/2}$ and Fe-$2p_{1/2}$ states of Fe(III), respectively.[6] The energy peak intensity of the iron elemental spectrum reveals that Fe(II) states are dominant as compared to Fe(III) and Fe(III) may remain as a residue during the reaction. The binding energy peak at 718.33 eV corresponds to the satellite peaks, which may be due to environmental oxygen or some residue of solvent linker during the reaction.[7] The elemental spectrum of carbon showed the binding energy peaks at 284.48, 286.10, and 288.24 eV (Fig. S2b). The peaks at 284.48 and 286.10 eV positions correspond to the C=C/C-C and C-N bonds of imidazole, respectively. In comparison, the peaks at position 288.24 eV suggest the oxidation of the electrocatalyst from the environment or maybe from the linkers.[8, 9] The nitrogen elemental spectrum showed the binding energy peaks at the positions of 396.01, 397.76, 398.92 and 400.20 eV (Fig. S2c). The binding energy peaks at 397.76, and 400.20 eV correspond to the pyridine and graphitic nitrogen.[8] Meanwhile, the binding energy peaks at the position of 398.92 eV reveal the orbital overlapping and coordination of metals (iron) with nitrogen in the imidazole.[3, 10-12]

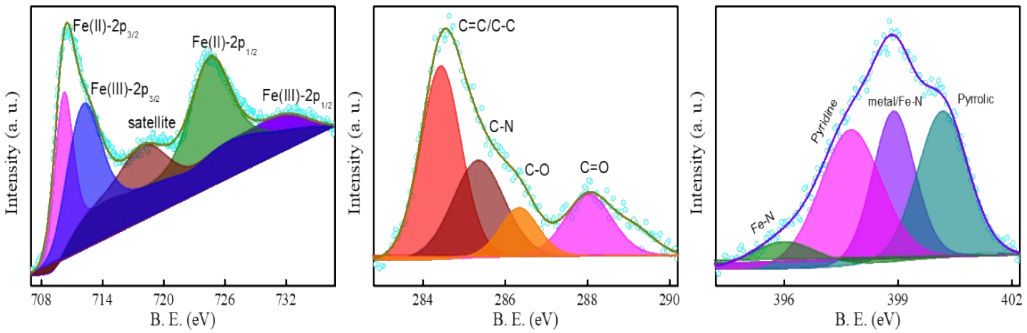


**Fig. S2.** XPS elemental spectrum of Fe@ZIF-67-1 (a) iron (b) carbon (c) nitrogen.

**3. Morphological analysis**

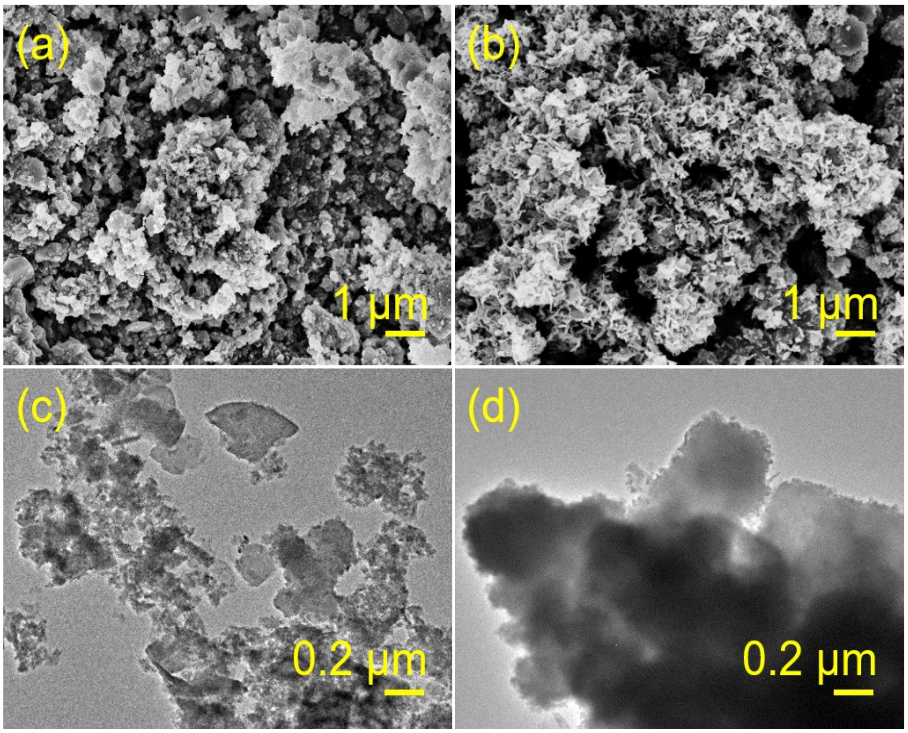


**Fig. S3.** SEM images (a) Fe@ZIF-67-1 (b) Fe@ZIF-67-2 structures and TEM images (c) Fe@ZIF-67-1 (d) Fe@ZIF-67-2 structures.

**4. HER activity**

**Table S2.** Summary of electrochemical parameters for the HER activity of the electrocatalysts.

| **Electrocatalyst** | **Electrolyte** | **Overpotential (mV)** | **Tafel slope (mV dec$^{-1}$)** | **TOF ($ms^{-1}$) at fixed 800 $mV_{RHE}$** |
|---|---|---|---|---|
| Fe@ZIF-67-1 | 1 M KOH | 75 | 83 | 108.23 |
| Fe@ZIF-67-2 | | 45 | 32 | 129.35 |
| Fe@ZIF-67-1 | 0.5 M $H_2SO_4$ | 256 | 227 | 96.80 |
| Fe@ZIF-67-2 | | 201 | 139 | 112.20 |
| | 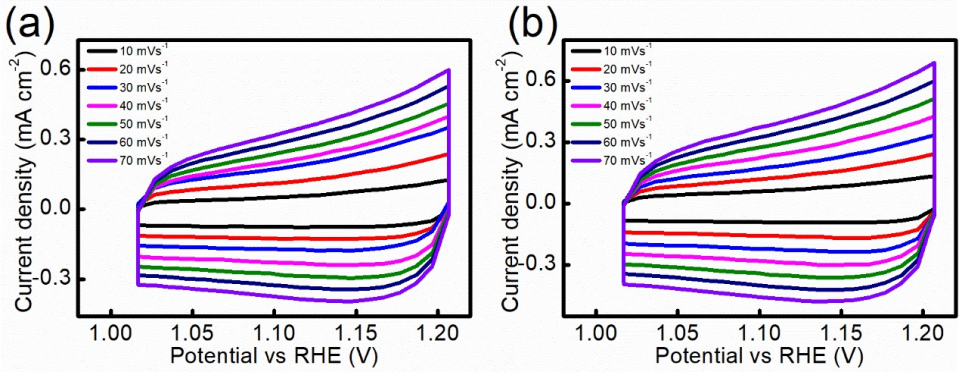 | | | |
| Fe@ZIF-67-1 | Seawater | 442 | 602 | 19.80 |
| Fe@ZIF-67-2 | | 402 | 550 | 25.10 |



**Fig. S4.** CV curves of (a) Fe@ZIF-67-1 and (b) Fe@ZIF-67-2 for ECSA in 1 M KOH.

**Table S3.** Summary of EIS parameters of the electrocatalysts.

| Electrocatalyst | Electrolyte | $R_s$ (Ω) | $R_{ct}$ (Ω) | C (F) | $J_{exc\ mA\ cm^{-2}}$ |
|---|---|---|---|---|---|
| Fe@ZIF-67-1 | 1 M KOH | 2.85 | 3.65 | $25.3 \times 10^{-4}$ | 7.04 |
| Fe@ZIF-67-2 | | 2.74 | 2.60 | $32.4 \times 10^{-4}$ | 9.90 |
| Fe@ZIF-67-1 | 0.5 M $H_2SO_4$ | 1.85 | 3.71 | $11.67 \times 10^{-6}$ | 6.92 |
| Fe@ZIF-67-2 | | 1.51 | 3.16 | $12.37 \times 10^{-6}$ | 8.13 |
| Fe@ZIF-67-1 | Seawater | 11.16 | 239.10 | $74.2 \times 10^{-6}$ | 0.11 |
| Fe@ZIF-67-2 | | 4.32 | 4955 | $1206 \times 10^{-6}$ | $5 \times 10^{-6}$ |

**5. References**


1. J. D. Benck, Z. Chen, L. Y. Kuritzky, A. J. Forman and T. F. Jaramillo, *ACS Catalysis*, 2012, **2**, 1916-1923.
2. X.-D. Wang, Y.-F. Xu, H.-S. Rao, W.-J. Xu, H.-Y. Chen, W.-X. Zhang, D.-B. Kuang and C.-Y. Su, *Energy & Environmental Science*, 2016, **9**, 1468-1475.
3. X. Shi, A. Wu, H. Yan, L. Zhang, C. Tian, L. Wang and H. Fu, *Journal of Materials Chemistry A*, 2018, **6**, 20100-20109.
4. M. H. Alkordi, J. A. Brant, L. Wojtas, V. C. Kravtsov, A. J. Cairns and M. Eddaoudi, *Journal of the American Chemical Society*, 2009, **131**, 17753-17755.
5. S. Ghoshal, S. Zaccarine, G. C. Anderson, M. B. Martinez, K. E. Hurst, S. Pylypenko, B. S. Pivovar and S. M. Alia, *ACS Applied Energy Materials*, 2019, **2**, 5568-5576.
6. L. Xiao, J. Han, Z. Wang and J. Guan, *International Journal of Hydrogen Energy*, 2023, **48**, 23776-23784.
7. C. Hu, H. Jin, B. Liu, L. Liang, Z. Wang, D. Chen, D. He and S. Mu, *Nano Energy*, 2021, **82**, 105714.
8. Y. Wang, Q. Du, H. Zhao, S. Hou, Y. Shen, H. Li, X. Kong, W. Sun, B. Zhang, S. Li, F. Huo and W. Zhang, *Nanoscale*, 2018, **10**, 17958-17964.
9. X. Yang, J. Cheng, X. Yang, Y. Xu, W. Sun and J. Zhou, *Chemical Engineering Journal*, 2023, **451**, 138977.
10. Y. Huang, W. Zhou, W. Kong, L. Chen, X. Lu, H. Cai, Y. Yuan, L. Zhao, Y. Jiang, H. Li, L. Wang, L. Wang, H. Wang, J. Zhang, J. Gu and Z. Fan, *Advanced Science*, 2022, **9**, 2204949.
11. Y. Liu, B. Zhou, Y. Zhang, W. Xiao, B. Li, Z. Wu and L. Wang, *Journal of Colloid and Interface Science*, 2023, **637**, 104-111.
12. Y. Liu, F. Lu, L. Yang, Y. Huang and Z. Hu, *Chemical Engineering Journal*, 2023, **471**, 144746.